Research Article Vol. 28, No. 2 / 20 January 2020 / Optics Express 1439
Optics EXPRESS

Impact of ship on radiometric measurements in the field: a reappraisal via Monte Carlo simulations

ZHEHAI SHANG,[1,*] ZHONGPING LEE,[1] JIANWEI WEI,[1] AND GONG LIN[2]

[1]School for the Environment, University of Massachusetts Boston, Boston, Massachusetts 02125, USA
[2]State Key Lab of Marine Environmental Science, Xiamen University, Xiamen 361005, China
[*]zhehai.shang001@umb.edu

Abstract: The presence of a ship in water disturbs the ambient light field and propagates errors to radiometric measurements. This study investigated the ship perturbation via Monte Carlo simulations with a reflective 3D ship. It is found that the height of ship could cause significant perturbation. However, these perturbations could be compensated by the reflection of the ship's hull, where such compensations vary from sun angle to hull's reflectance. Further, as a rule of thumb, to keep the perturbation on water-leaving radiance under ~3% from an operating ship, a look-up table is generated with the requirements of viewing angle for the radiometers operated at the deck and for the deployment distance of floating and profiling instruments.

1. Introduction

Ocean color is an indicator of constituents in water, where their spatial and temporal variations are of great importance for ocean biology and the ecosystem as a whole. The spectrum of ocean color is commonly described by remote sensing reflectance (R_{rs}, sr^{-1}), which is defined as the ratio of water-leaving radiance (L_w, W m^{-2} sr^{-1}) to downwelling irradiance just above the surface ($E_d(0+)$, W m^{-2}). Through empirical or semi-analytical inversion of an R_{rs} spectrum, waters' inherent optical properties (IOPs) and/or concentrations of chlorophyll can be derived. Because of this, ocean color satellites have been launched and operated to provide synoptic measurements of chlorophyll for the global ocean [1–6]. These data are further applied for the estimation of primary production [1,7–9] and monitoring of harmful algae blooms [1,10–13].

Either for the development of remote sensing algorithms [14–23] or for the validation of satellite R_{rs} products [24–28], accurate field measurements of R_{rs} are required. Usually such field activities involve a ship as the operation platform. Over the past decades, the ocean color community have used Above-Water (AW) and In-Water (IW) approaches to obtain R_{rs} in the field. The AW approach is usually carried out by operating radiometric instruments on board a ship [29,30]. $E_d(0+)$ could be acquired in two ways for AW approaches [31], with the most straightforward way to point an irradiance sensor looking upward to the zenith. The other is to measure the radiance reflected from a standard plaque, with $E_d(0+)$ calculated based on the measured radiance and the reflectance of the plaque. For the L_w measurement, it is carried out by pointing the radiance sensor toward the water to get the upwelling radiance above the surface ($L_u(0+)$). The water surface reflected light (L_{sr}, W m^{-2} sr^{-1}) is removed by various schemes [26,30,32] and L_w is calculated from $L_u(0+)$.

The IW approach involves deploying instruments over the side of the ship and these instruments are equipped with a radiance sensor pointing downward and an irradiance sensor pointing upward. Generally, there are two ways to measure L_w and $E_d(0+)$. The first IW approach is carried out by deploying a surface floating platform, equipped with radiance and irradiance radiometers pointing downward and upward, respectively. The upwelling radiance obtained from the radiometer

#366458 https://doi.org/10.1364/OE.28.001439
Journal © 2020 Received 1 May 2019; revised 28 Aug 2019; accepted 2 Sep 2019; published 10 Jan 2020

Optics EXPRESS

depends on the design of the platform. It could be measured from a few centimeters below the surface (L_u(z), W m^{-2} sr^{-1}) (e.g., the Tethered Spectral Radiometer Buoy (TSRB: Satlantic Inc. [33])) or a few centimeters above the surface (L_w) (e.g., the Skylight-Blocked Approach (SBA) [34]). For the L_u(z) measured below surface, it can then be propagated to L_w later by applying the correction for crossing the water-air interface. The E_d(0+) can be directly measured by an irradiance sensor. The other IW approach is to cast a free falling profiler (e.g., Hyperpro [35]) that measures upwelling radiance (L_u(z), W m^{-2} sr^{-1}) and downwelling irradiance (E_d(z), W m^{-2}) in water. The attenuation for L_u(z) and E_d (z) can then be estimated; further L_u(0-) and E_d(0-) (downwelling irradiance just below the surface), respectively, are calcualted from L_u(z) and E_d(z). After that, r_{rs} (remote sensing reflectance just below the water surface) can be calculated and R_{rs} could be estimated by implementing a cross surface conversion.

The presence of an operating ship in water, however, will disturb the ambient light field by either blocking a portion of the light from the sky (sky shadow of the ship) or reflecting sun light by the ship's hull. Consequently, there will be uncertainties in the measured radiance and irradiance, which further propagate to the calculated R_{rs}.

The ship perturbation on the ambient light field was first investigated by Gordon [36] using numerical (Monte Carlo) simulations. In that work, for easier simulation and aimed at the profile of downwelling irradiance (H. Gordon, personal communication), the "ship" was set as a 2D black sheet (38.4 m by 6.55 m) without a hull or superstructure. It was found that if radiometers are about 1.5 m away from the ship, the perturbation to E_d(z) is within 5% for waters with an attenuation coefficient (c, m^{-1}) as 0.1 m^{-1} and under a clear sky. The perturbation will be reduced for lower sun elevations or the sensors are deployed further away from the ship. More perturbations will be introduced to E_d(z) if the relative contribution from the diffuse skylight (E_{d_dif}, W m^{-2}) increases.

Later, Piskozub [37] conducted more Monte Carlo (MC) simulations aimed at the combined impact of ship and surface roughness on the profiles of downwelling and upwelling irradiance. In these MC simulations, a 3D ship was used, but the ship was black and had no superstructure above the sea surface [37]. In addition, the simulation setup assumed a black sky (i.e. $E_{d\_dif} = 0$). The results from these simulations indicated, as would be expected, an increase of ship size will have larger impact on the upwelling irradiance. Also, the results indicated that varied surface roughness causes no significant impact on irradiance perturbation from the ship. These results, however, are far from realistic field and ship conditions where there are strong contributions from the sky (especially in blue wavelengths) and a ship is rarely black. More importantly, there are superstructures above the sea surface (ship height) which are not considered in Piskozub's simulations [37].

Zibordi *et al.* [38] and Doyle and Zibordi [39] later used MC simulations to evaluate the perturbation (shading error) to the ambient light field caused by a tower (12.3 m by 7 m by 5 m), which is a platform with superstructure above the surface (along with underwater tower legs). These works investigated the perturbation of this tower to instruments deployed at a distance from 2.5 to 22 m from the tower. Results from both studies showed that the perturbation of this tower on the upwelling radiance and the downwelling irradiance declines when 1) skylight contribution decreases, 2) instruments are further away from the tower, and 3) the absorption coefficient of the water becomes higher. These results provide insight on perturbations of the light field from a 3D structure, but not necessarily matching that of an operating ship because the tower's shaped structure and reflection was not accounted for.

There have also been investigations via field measurements to characterize the perturbation due to the presence of a ship (Voss *et al.* [40], Spinrad *et al.* [41] and Weir *et al.* [42], Hooker and Morel [43]). Specifically, in Voss et al, the investigation was made with a profiler deployed very close to a ship (ship *R/V Weatherbird II*, with size 35 m by 8 m by 2.6 m) and deployed 9 m away from the ship. Based on the difference of the measured radiance and irradiance from these

Optics EXPRESS

two deployments, the ship perturbation is calculated. It is found that under a clear sky with solar zenith angle around 40°, the perturbations on $E_d(412)$ and $L_u(412)$ at 1 m depth are around -2 to -8% and -2 to -12%, respectively. Under overcast sky, the perturbation on E_d and L_u became -30 to -40% for wavelengths between 410 nm and 673 nm. These results were later supported by measurements from Weir *et al.* [42]. Using submersible platforms, Spinrad *et al.* [41] showed that for the ship Edwin Link (around 51 m long), the error in measured photosynthesis available radiation (PAR) in the upper 20 m is around -5% for a PAR sensor within 10 meters of the ship and on the sunny side (solar zenith angle varies from 36° to 61°).

In addition, Hooker and Morel [44] examined ship (*Thalassa*, with a size 74.5 m by 13.9 m by 6.2 m) perturbations on both AW and the IW approaches to measure water-leaving radiance in "case-1" waters under a clear sky (solar zenith from 33° to 50°). The IW measurements were taken with instruments deployed 30 to 50 m away from the ship and found that the absolute perturbation on the water-leaving radiance was within 5%. However, the perturbation on L_w could be as high as 27% by the above-water approach if the viewing angle is 20° from the nadir.

The above measurements and numerical simulations all show the substantial impact of an operating ship on the ambient light field and remote sensing reflectance, and indicates it is better to deploy measurement instruments as far as possible from the ship. However, for field measurements, it is challenging to deploy instruments 100's of meters away from the ship. It would be useful to provide a practical guidance on the minimum distance from the ship, minimum viewing angle from nadir for above-water measurements, and where the ship perturbation can be considered acceptable. This is especially vital where many measurements were carried out with a large-size non-black operating ship, such as the Okeanos Explorer (Fig. 1(a)) operated by NOAA, which has a size of 60 m by 15 m by 10 m, with a ship hull to reflect light. It is not known how far away or how large the angle the measurement can be considered "safe", a conclusion not available from previous studies.

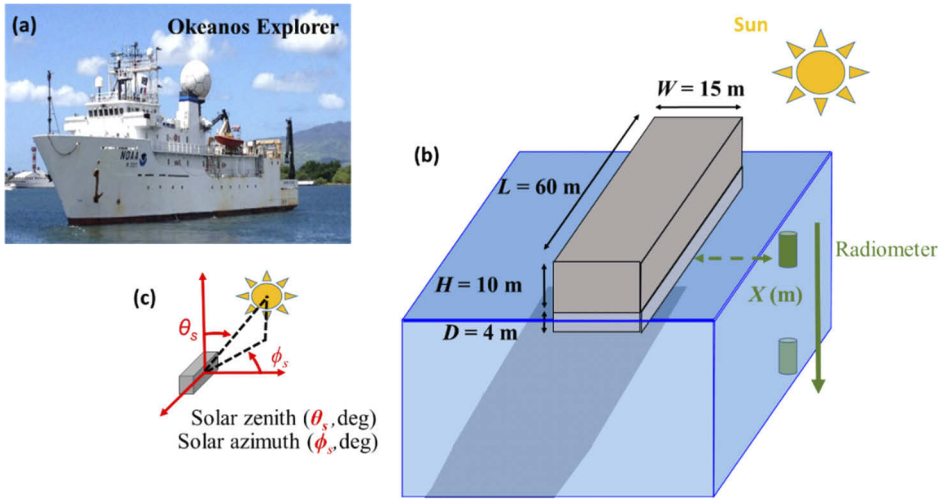

Fig. 1. The cubic ship (a) and the geometry setting ((b) and (c)) in this study.

Thus, there are two objectives in this study. The first objective is to fill this gap by investigating the change of light field for different waters and solar illuminations when there exists a 3D sized shape with hull reflectivity. In particular, in addition to common parameters such as distance from the ship and sun angle etc., we evaluate the impact of ship's height and reflectance on this perturbation. The second objective is to provide a general guidance on field measurements of radiance and irradiance when a ship is used as the operating platform. We investigate the

Optics EXPRESS

perturbations under the common conditions of field radiometric measurements and a look-up table is generated, which helps reducing ship perturbation when deploying instruments from ships.

2. Setup of Monte Carlo simulations

2.1. Configuration of the "ship"

To simplify the calculation but not lose generality, the ship is set as a cube shape as in Piskozub [37], but with both superstructure and draft. The ship dimensions are set in reference to Okeanos Explorer (Fig. 1(a)) [45] with sizes as 60 m in length (L), 15 m in width (W) and 10 m in height (H) (the part above the waterline, see Fig. 1(b)). The draft (D) is set as 4 m. To better present the reflected perturbation of the ship, the reflectance of ship's hull (R_{hull}) and draft (R_{draft}) are both set as 20%, respectively. The geometry applied in this study is shown in Figs. 1(b) and 1(c).

2.2. Configuration of sky and water properties

The illumination assumed in the model consists of two light sources: beam illumination from the Sun and the diffuse illumination from the sky. The skylight is assumed to be isotropic, with its irradiance represented as part (r_{sky}, in percent) of the total downwelling irradiance (the sum of the beam and the diffuse downwelling irradiance).

Water is considered homogenous and optically deep, with the Fournier-Forand model for scattering phase function [46,47]. Fluorescence from chlorophyll and colored dissolved organic matter are excluded for efficient calculations as in earlier studies [36,37,43].

Following Gordon [36] and Leather's *et al.* [48], a backward MC scheme developed in Shang *et al.* [49] is adopted for this study. The tracing process of photons starts from the receiving side (i.e., radiometer) and it ends if the intensity of the photons is too low or the photon hits the sky (the illumination source). This simulation system for a 3D light field in water was verified with Hydrolight simulations.

2.3. Geometry of sensors

Radiometers for radiance and irradiance are deployed on the sunny side of this "ship" to ensure minimal sun shadow from this ship. In-water instruments are deployed at the side of the ship to enhance the perturbation and make the perturbation patterns comparable to earlier studies, and easy to be characterized. A value (X) is used to measure the horizontal distance of this instrument from this ship (Fig. 1).

2.4. Radiometric quantities

The perturbation is evaluated based on the impact on four radiometric parameters (RP), which are water-leaving radiance at zenith angle (L_w), upwelling radiance (zenith angle is 0°) in water (L_u(z)), downwelling irradiance above surface (E_s) and downwelling irradiance in water (E_d(z)), respectively.

The perturbation of each RP (ε_{RP}) is defined as:

$$\varepsilon_{RP} = \frac{RPs(ship) - RPs(no\ ship)}{RPs\ (no\ ship)} * 100\% \tag{1}$$

The RPs from right above the surface to a depth of 60 m, with and without the presence of this ship, are simulated and compared.

2.5. Consistency check on MC simulations

We first compared the resulted ε_{Eu}(z) (E_u: upwelling irradiance) and ε_{Ed}(z) with the same setup on illuminations and IOPs as that in Piskozub [37] for a consistency check, where the "ship"

Optics EXPRESS

is black without a hull, and Fig. 2 shows the comparison. The results indicate that $\varepsilon_{Eu}(z)$ and $\varepsilon_{Ed}(z)$ obtained from both Piskozub's simulation and this study under identical settings agree with each other excellently (the difference is < 1% for $\varepsilon_{Eu}(z)$ and < 0.3% for $\varepsilon_{Ed}(z)$). The small difference is most likely related to differences in computer architecture and programming [50]. Such results provided us with confidence in the MC code and allowed us to investigate the impact of a more realistic ship on both irradiance and radiance fields, especially the upwelling radiance and water-leaving radiance, which is critical for remote sensing.

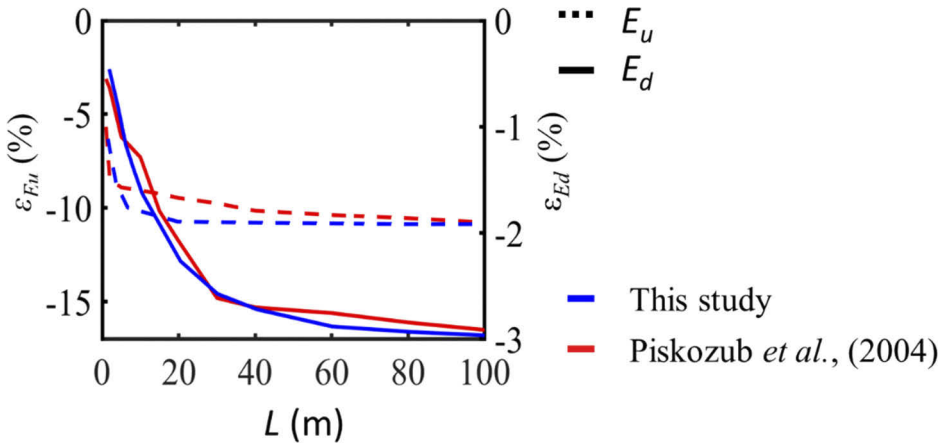

Fig. 2. Comparison of E_d and E_u perturbation patterns (absorption coefficient = 0.1 m^{-1}, scattering coefficient = 0.25 m^{-1}, at 10 m depth with a ship of 9 m draft).

2.6. Parameters evaluated for ship perturbation

To characterize the patterns of the perturbation, the following parameters are considered and evaluated in relationship to ship perturbation:

(1) Illumination parameters, which include the solar zenith angle (θ_s) and the diffuse illumination ratio (r_{sky}).

(2) Horizontal distance from the ship (X).

(3) Ship height. The height of the ship ranges from 1 m to 20 m. Besides, the default reflectance of ships' hull (R_{hull}) and draft (R_{draft}) is set as 20%.

(4) IOPs of the aquatic environment, which consist of absorption coefficient (a), scattering coefficient (b) and the backscattering coefficient (b_b). In this study, a varies from 0.05 to 2.0 m^{-1}, b varies from 0.1 to 1.5 m^{-1}, b_b varies from 0.001 to 0.015 m^{-1}, these IOPs cover both oceanic and coastal water properties.

Unless further specified, the default values for the above listed parameters used in the simulations are presented in Table 1.

Optics EXPRESS

Table 1. Default value of parameters in MC

a	0.1 m^{-1}	R_{hull}	20%
b	0.1 m^{-1}	R_{draft}	20%
b_b	0.001 m^{-1}	X	2 m
L	60 m	r_{sky}	25%
W	15 m	θ_s	30°
H	10 m	ϕ_s	0°
D	4 m		

3. Results

As would be expected, the impact of a ship on the radiance and irradiance field is quite complex. This is a result of the ship's size and reflectivity, optical properties of the water and the sun and skylight contributions. For easier characterization and interpretation, the impact of a ship on the radiance and irradiance field for the various parameters are described below separately.

3.1. Illumination parameters

Two illumination parameters are considered, one is the solar zenith angle, another is the relative contribution of the diffuse skylight, with ε_{Es}, ε_{Lw}, ε_{Ed}(z) and ε_{Lu}(z) presented in Figs. 3 and 4. Overall, values of ε_{Es} and ε_{Ed}(z) are negative for low sun zenith angles (see Fig. 3(a)), indicating a reduction of downwelling irradiance due to the presence of a ship. This result is generally consistent with earlier simulation results, although the actual quantitative value will be different due to different setups [36]. Also, for E_s and even the sun is at the zenith, ε_{Es} (with $X = 2$ m) can be as low as -7%, a result due to the blocking of skylight by the ship's superstructure. On the other hand, apparently due to reflection by ship's hull (R_{hull} 20% for this case), values of ε_{Es} and subsurface ε_{Ed}(z) become positive when θ_s exceeds 30°. These findings expand earlier studies on ship perturbation when a more realistic "ship" is considered. Also, consistent with earlier results [36,37], the presence of a ship resulted in negative values of ε_{Es} and ε_{Ed}(z) for a diffuse skylight (see Fig. 4(a)), especially if this contribution is strong.

As a result, from ship's reflection ($R_{hull} = 20\%$, $R_{draft} = 20\%$) and ship's height, solar zenith angle brings less negative (or more positive) perturbation to E_d(z) (Fig. 3(a)). This pattern is a result of the combined effects of two factors: 1) higher solar zenith angle increases the reflected light by ship's hull and draft, which then compensates the sky shadow, and 2) ship causes less sun shadow when solar zenith angle increases, thus reduce negative perturbation.

Because r_{sky} is wavelength dependent, Fig. 4(a) implicitly also shows a spectral variation of ε_{Ed}(z), where ε_{Ed}(z) becomes positive for low r_{sky} (red wavelengths) and high reflectance of the ship's hull. For blue wavelengths where r_{sky} values are generally higher, there could be a significant negative impact on E_d(z) (see Fig. 4(a)).

Generally, ε_{Lu}(z) has a similar pattern as ε_{Ed}(z) (Figs. 3 and 4), although the values are slightly different. On the other hand, ε_{Lw} can be very different from ε_{Es}. For instance, when the sun is 60° from zenith, ε_{Lw} is ~6%, while ε_{Es} is ~2%. This is because the E_s is a measurement of downwelling light while the L_w is a measurement of upwelling light. The majority of the downwelling illumination above the surface is contributed by the collimated beam from the Sun.

3.2. Reflection from ship's hull

The presence of the ship does not block the direct path of the dominated illumination from the Sun to the E_s sensor, but reflection from ship's hull brings positive perturbation by reflecting sun and sky light, which compensates to some degree the sky shadow.

Optics EXPRESS

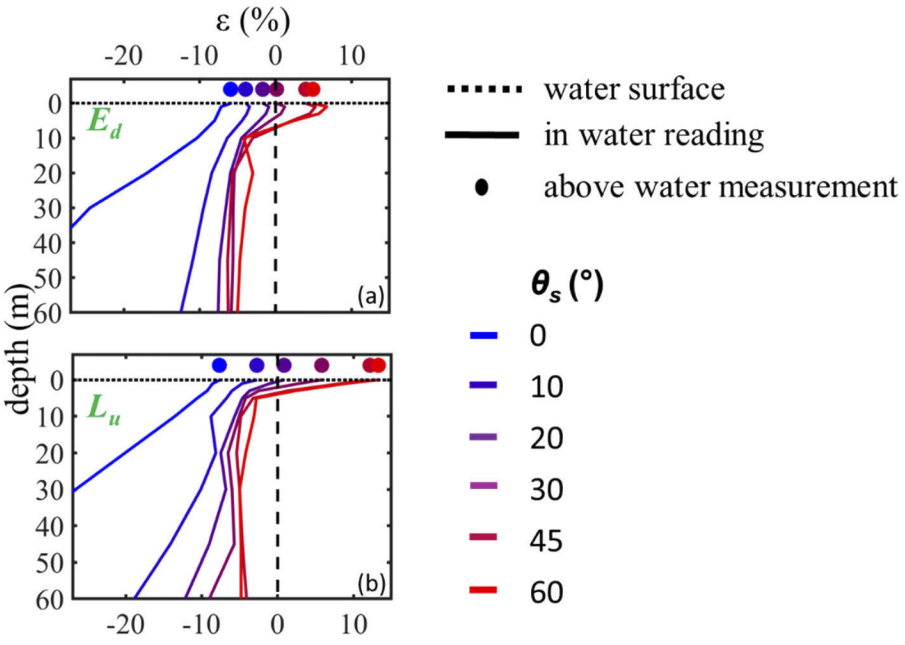

Fig. 3. Perturbation patterns for different solar zenith angles ($r_{sky} = 25\%$; $X = 2$ m).

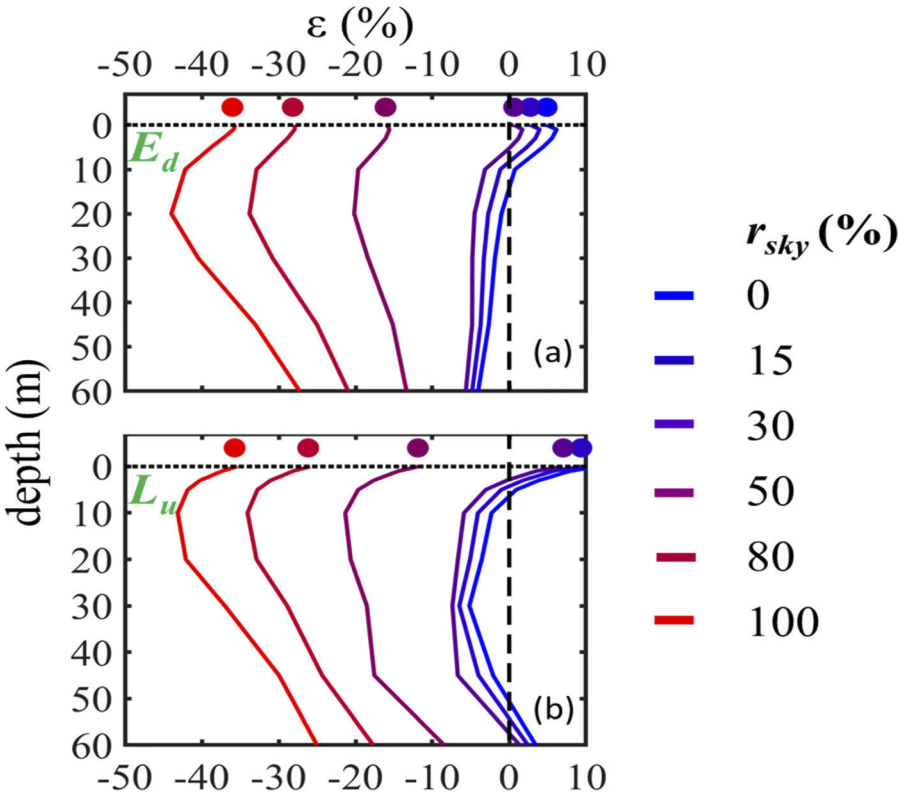

Fig. 4. Perturbation patterns for different contributions of diffuse light ($X = 2$ m; $\theta_s = 30°$).

Optics EXPRESS

L_w, on the other hand, is determined by the upwelling light transmitted from the water column. The intensity of upwelling light within the water column at a certain depth is contributed by two sources. The first one is the light transmitted from photons at deeper depths, which is strongly related to the attenuation coefficient of the water. Another one is the downwelling light being backscattered at this depth. In this case, when r_{sky} is low (e.g., no more than 30%), which means the major downwelling illumination comes from the direct solar beam, 0.01 backscattering ratio (b_{br}) makes around 1% of the downwelling illumination goes upward when a scattering process happens. When a ship is present, the light going upward will include those from the ship's reflection. With $R_{draft} = 20\%$ and a Lambertian surface for ship's surface, 10% of the light hitting ship's surface goes upward. Compared with contributions from water's backscattering, reflection by ship's draft could contribute significantly to the upwelling radiance if the radiometer is close to this ship ($X = 2$ m). Consequently, a positive perturbation is much stronger on L_w than on E_s for low r_{sky} ($r_{sky} \leq 30\%$).

3.3. Distance off the ship

The distance of a profiling instrument from an operating ship was a question raised long ago [25,36,51], and various studies have addressed this question using numerical simulations and field measurements [36,37,40–42,51,52]. Figure 5 presents results of $\varepsilon_{Lu}(z)$ and $\varepsilon_{Ed}(z)$ for different X values in this study. For both clear sky (Sun at 30° from zenith) and overcast sky, ε_{Es} is negative due to the superstructure (close to 0% for clear sky with θ_s as 30°). Also, as expected, values of $\varepsilon_{Ed}(z)$ become smaller (less impact) if the instrument is farther away from the ship. This impact on E_s will be < 1% if the distance is 20 m away from this ship for clear sky condition, but about ~3% if it is overcast sky for the same distance.

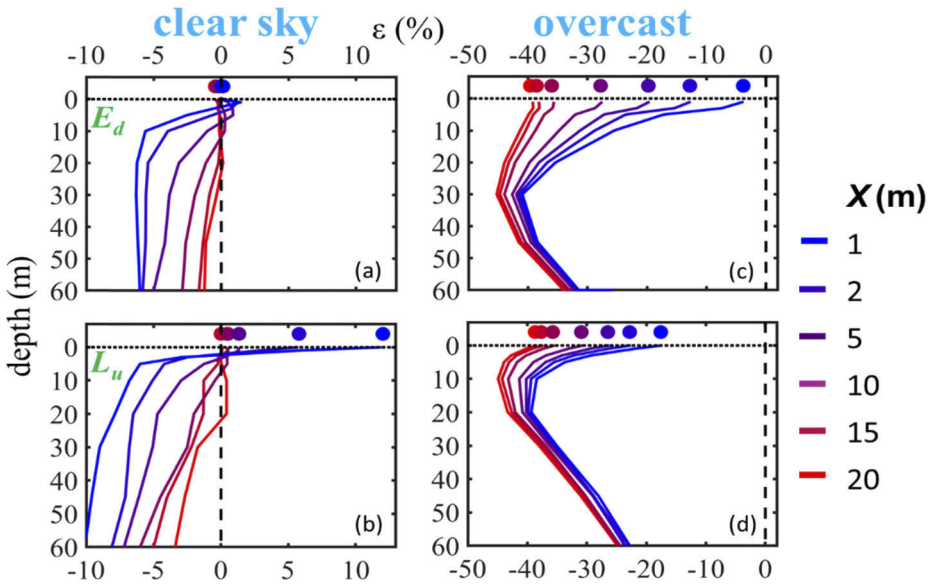

Fig. 5. Perturbation patterns for different distance from the ship ($\theta_s = 30°$, $r_{sky} = 25\%$).

The value of $|\varepsilon_{Lu}(z)|$ is around 2% even for clear sky conditions with a distance 20 m away from such a ship, which suggests a non-negligible error source for *in situ* measurement of L_w if a highly accurate measurement is desired. More importantly, ε_{Lw} can be >10% for clear sky condition (Fig. 5(b)) while about -35% for overcast condition (Fig. 5(d)) if the distance is 1 m away, indicating complex impact of the reflective hull on the upwelling light field. Such results

Optics EXPRESS

further indicate the importance of keeping the radiometers far away (i.e., ≥ 20 m or further for a ship size like Okeanos Explorer [45] under such conditions (e.g., r_{sky} and IOPs)) for accurate measurements of radiance and irradiance.

For all X values considered, the negative impact on both $\varepsilon_{Lu}(z)$ and $\varepsilon_{Ed}(z)$ increase with deeper depth under clear sky for such a ship. Generally, $|\varepsilon_{Ed}(z)|$ is under ~5% and $|\varepsilon_{Lu}(z)|$ is less than ~10%. However, $|\varepsilon_{Ed}(z)|$ and $|\varepsilon_{Lu}(z)|$ could be as much as 40% under the overcast sky. In general, as expected, the impact decreases with the increase of distance (X). These values are higher than previous numerical studies [36,37] due the setup of a more realistic ship.

3.4. IOPs

The light field in water is highly dependent on water's IOPs. Therefore a wide range of impact is found on both radiance and irradiance fields due to the existence of this ship (Figs. 6 and 7). Because radiance (or irradiance) attenuates exponentially with depth, the light intensity is very low at deeper depths when the attenuation is strong. Consequently, the resulted $\varepsilon_{Lu}(z)$ and $\varepsilon_{Ed}(z)$ at those depths under high attenuation (e.g., $a > 0.5\ m^{-1}$) suffer considerable noise and offer no help for characterizing the patterns of perturbation; thus they are not presented in the following (including Figs. 6(a), 6(d), 7(a) and 7(d)). Generally, it is found that:

(1) $|\varepsilon_{Lu}(z)|$ and $|\varepsilon_{Ed}(z)|$ decrease with the increase of a. This is because when absorption coefficient increases, the contribution to $E_d(z)$ from the shadowed area decreases (especially under clear sky conditions). For ε_{Lw}, however, it is quite complex. The value of ε_{Lw} can be low for both high and low absorption coefficients when the sky is clear, which is a result of L_w originating from the entire upper water column. For low absorption coefficient, there are more contributions from deeper waters where a ship causes relatively less perturbation to the light field. On the other hand, for high absorption coefficient, most of the upwelling light is generated from backscattering in near surface waters and is thus less dependent on the contributions from the ship-blocked areas.

(2) $|\varepsilon_{Lu}(z)|$ and $|\varepsilon_{Ed}(z)|$ slightly increase with b. For given absorption and backscattering coefficients, higher b would increase the contributions of photons to $E_d(z)$ from the areas the ship occupied (reflected and/or blocked). When a ship is present, this portion of photons contributing to $E_d(z)$ are eliminated; consequently, resulting in losing more of photons and then higher $|\varepsilon_{Lu}(z)|$ and $|\varepsilon_{Ed}(z)|$ values (Figs. 6(b), 6(e), 7(b), and 7(e)), although the difference is not significant. Also, there is almost no impact to $|\varepsilon_{Lw}|$ for the varying b values, mainly because L_w is determined by incident radiation, absorption and backscattering coefficients, and not the forward scattering coefficient (which makes ~98% of the scattering coefficient).

(3) It is interesting, and somewhat surprising, that $|\varepsilon_{Lu}(z)|$ and $|\varepsilon_{Ed}(z)|$ clearly increase with b_b, especially at deeper depths (i.e., more than 20 m deep). This is likely because that based on the two-stream radiative transfer model (Aas [53]), backscattering is an important component for both the upwelling and downwelling light streams. The presence of a ship will disturb this contribution to $E_d(z)$ and $L_u(z)$, and the higher the b_b value, the larger the loss of this component, and then higher impact. This is further echoed in the value of ε_{Lw}, which decreases with higher b_b value (from ~5% to ~ -2% for b_b from 0.001 to 0.01 m^{-1} under the clear sky) for these simulation setups. These results expand our knowledge of IOPs related ship perturbation, as previous numerical simulations did not investigate the relationships between ship perturbation and backscattering coefficients.

Optics EXPRESS

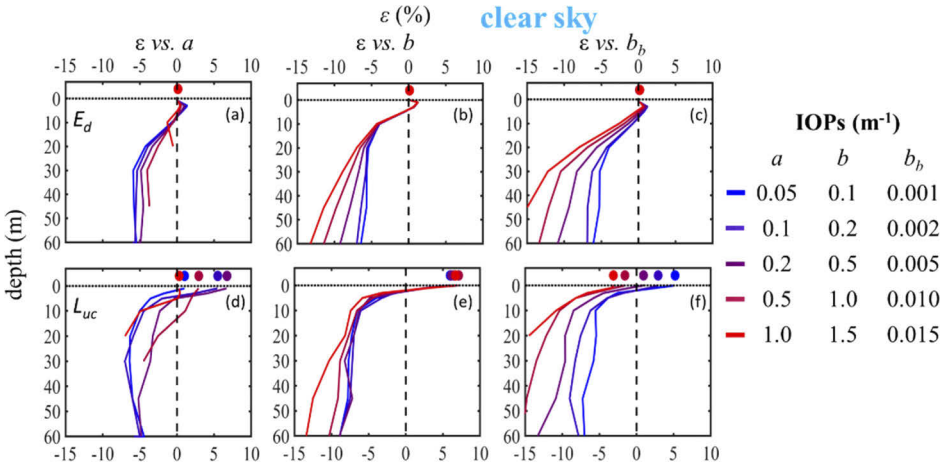

Fig. 6. Perturbation patterns for different IOPs under clear sky ($\theta_s = 30°$, $r_{sky} = 25\%$, $X = 2$ m).

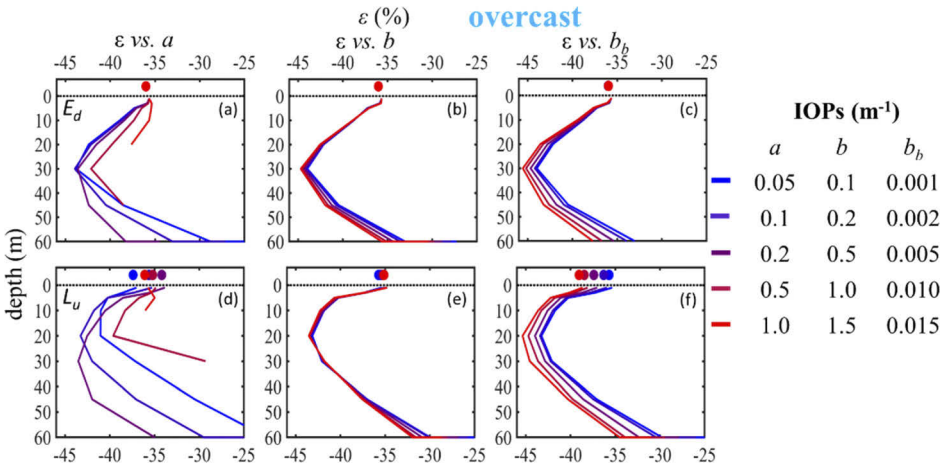

Fig. 7. Perturbation patterns for different IOPs under overcast sky ($r_{sky} = 100\%$, $X = 2$ m).

3.5. Ship height

An important aspect of this effort is to characterize the impact of ship's height on radiance and irradiance measurements, with results presented in Fig. 8. To highlight the impact due to this superstructure, for clear sky conditions, the solar zenith angle is set at 60°.

3.5.1. Under clear sky ($\theta_s = 60°$, $r_{sky} = 25\%$)

For a ship height of 20 m under clear sky conditions, $|\varepsilon_{Ed}(z)|$ and $|\varepsilon_{Es}|$ can be as high as ~7% with most of the variation found in $|\varepsilon_{Es}|$. On the other hand, values of $|\varepsilon_{Lu}(z)|$ and $|\varepsilon_{Lw}|$ can be greater than 10% even for a ship height of 1 m ($X = 2$ m). With increasing depth, the change of ship height only slightly alters the sky shadow, especially under a clear sky (Figs. 8(a) and 8(c)). These results show that upwelling radiance, including L_w, is very sensitive to ship height, as most of the photons are coming from the upper layer. It also suggests caution is necessary when analyzing historical measurements where often radiometers were operated right beside an operating ship.

Optics EXPRESS

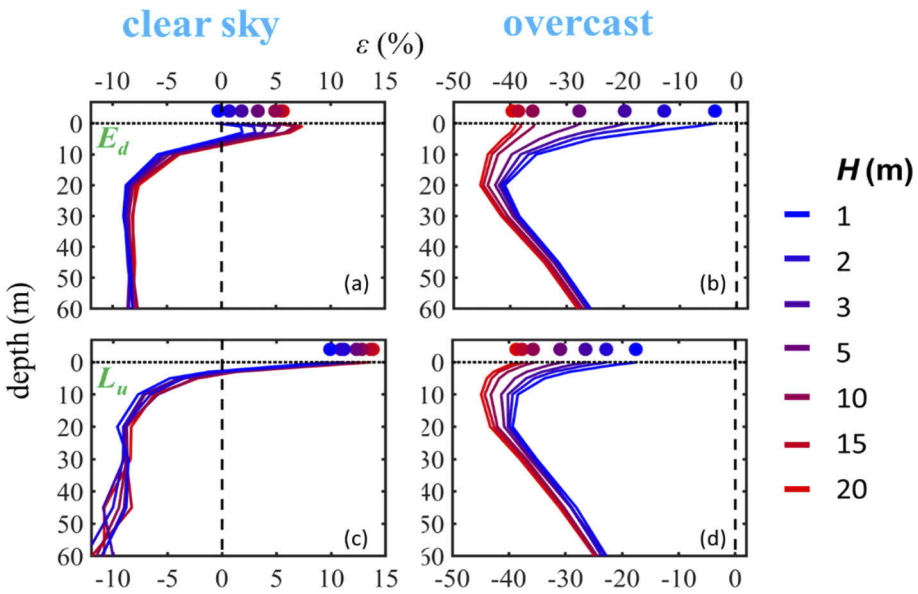

Fig. 8. Perturbation patterns for different ship height ($\theta_s = 60°$, $r_{sky} = 25\%$, $X = 2$ m).

3.5.2. Under overcast sky ($r_{sky} = 100\%$)

As expected, because the diffuse skylight is the source of illumination, there are significant impacts on both upwelling radiance and downwelling irradiance due to ship height, with $|\varepsilon_{Lw}|$ and $|\varepsilon_{Es}|$ as high as 40%. Also, this impact increases with the ship height, as it will block more light from the sky. Again, there are peaks for $|\varepsilon_{Lu}(z)|$ and $|\varepsilon_{Ed}(z)|$, resulted from the maximum solid angle formed between the point of sensor and the size of this ship that is discussed earlier. Further, the vertical patterns of $|\varepsilon_{Lu}(z)|$ and $|\varepsilon_{Ed}(z)|$ gradually converge with depth (e.g., around 25% at 60 m depth) (Figs. 8(b) and 8(d)).

4. Discussion

4.1. Ship perturbation under various conditions

Based on the results presented above, the sky contribution is a major factor in ship perturbation, as conventionally all radiometer sensors are in the sunny side, so there is only a sky shadow by the operating ship. Because of this sky shadow, a ship (such as Okeanos Explorer) can bring ~ 30% or more negative perturbation for overcast sky. Although generally there will be measurements of optical and other parameters in the field regardless of the sky conditions, the discussion below focuses on the perturbation under clear sky ($r_{sky} = 25\%$) as it is the condition to obtain a good matchup between field and satellite measurements.

One of the critical variables of this study, ship height, is found to result in a 5% difference for all ε_{RPs}, with H from 1 to 20 m for the upper 5 meters layer ($X = 2$ m, $R_{hull} = 20\%$, $R_{draft} = 20\%$, $\theta_s = 60°$, $r_{sky} = 25\%$). This is a consequence of the positive perturbation from ship's hull and draft and the negative perturbation by the ship blocking diffuse skylight. The perturbation on $L_u(z)$ ($z < 3$ m) and L_w is mostly contributed by the reflected light of the ship draft. In this case, the ship hull/draft with a 20% reflectance provides a considerable boost (around 10 to 15%) to L_w when the sun is at 60° from the zenith.

Another key factor, the distance off ship (X) is vital for accurate measurements of radiance and irradiance. Under the considered parameters (ship size, IOPs and r_{sky}) in this study, it shows that

Optics EXPRESS

if the sensor is deployed 20 m away from the ship, the $|\varepsilon_{RPs}|$ could be limited to around 2.5% or close to zero from the above surface to 60 m depth.

Previous studies [36,37] show that an increase of θ_s will reduce ship's negative perturbation. However, those studies assumed a flat ship along with fixed contributions from the diffuse skylight. Here we found that for a ship with a 3D superstructure and a reflective hull, a specification closer to reality, the ε_{Es} and ε_{Lw} shifts from -6% and -8% to 5% and 12% ($X = 2$ m), respectively, when θ_s increases from 0° to 60°. These results emphasize the importance of avoiding ship's superstructures when conducting out field radiometric measurements.

4.2. Implication to radiometric measurements in the field

Due to the complexities of ship perturbation on the ambient light field, it is of more value to develop criteria for minimizing ship perturbation on radiometric field measurements. For this purpose, a "case-1" water with chlorophyll concentration equal to 0.1 mg m^{-3} is chosen for another batch of MC runs. The simulation covers wavelengths from 350 nm to 700 nm, with detailed information presented in Table 2, and the cubic ship with same dimensions as in Fig. 1(b), but with different reflectivity on ship draft ($R_{draft} = 5\%$). A wavelength-dependent sky contribution (spectral r_{sky} is calculated based on the clear-sky model in Gregg et al. [54]) and $\theta_s = 30^o$ as the illumination conditions are considered. To match the realistic deployment, unlike the previous section, the IW instruments are assumed to be deployed off the stern while the AW measurements are also assumed taken at the stern (Fig. 9(a)). X_s is the horizontal distance between the IW instruments and the stern. Besides, both measurements are at the sunny side of the ship. Results of the perturbation on *RPs* for AW and IW approaches are summarized below (Table 3):

(1) From the AW approach, L_w and E_s are usually measured over the side or on the bow of an operating ship [27]. The perturbation on E_s in this scenario is negligible as it is assumed that no superstructure is above the measurement height for E_s. To account for this, for the simulated AW measurements, it is assumed that the sensors are on the sunny side (~90° azimuth relative to the sun) and close to the stern as illustrated in Fig. 9(a). It needs to be noticed that conventionally, the AW measurements are taken on the bow of the ship (e.g., Hooker and Morel [43]). While for this cubic ship, there is no difference between the stern and the bow. For L_w, it was found that low viewing zenith angle ($\theta_v = 10°$) introduces considerable perturbations (around -8.5% at 350 nm) (Fig. 9(b)). This is because the photons contributing to L_w are very close (about 1.8 m) to the operating ship, where a significant portion of the upwelling photons are blocked by the ship. The $|\varepsilon_{RPs}|$ can be kept under 3% if θ_v is 60° (equivalent X is 17 m). There is no apparent difference (Fig. 9(c)) from viewing azimuth angle (0° to 75°), as long as the sensor is kept away from the sun glint.

(2) The perturbation of IW approach for the same "case-1" water is presented in Fig. 10. For the IW approach, if the sensors are deployed 30 m away from the ship (with a size as Okeanos Explorer), the absolute perturbation is within 2.5% for L_w (and L_u) and E_s (and E_d) (Figs. 10(c) and 10(d)).

4.3. Minimum X_s and θ_v for measurement of L_w

In field measurements, size and reflectivity of an operation ship vary. To obtain a more practical guidance on the distance to cast instruments away from the ship or the view-zenith angle when viewing water at the 45° from the stern the ship ($\phi_v = 45°$), more MC simulations focused on L_w were conducted.

Optics EXPRESS

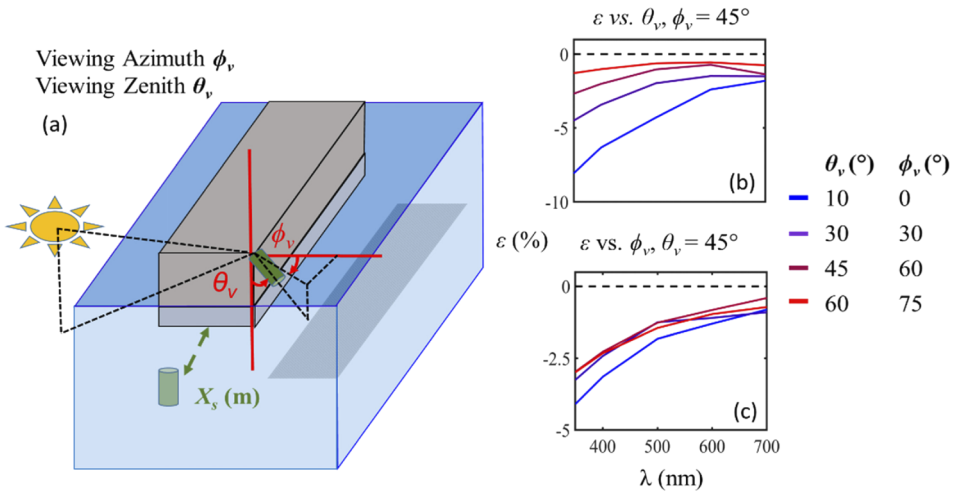

Fig. 9. Perturbation for AW measurements under the water with 0.1 mg m^{-3} chlorophyll concentration and the geometry setting ($\theta_s = 30°$; For AW measurements, $\phi_s = 90\text{-}165°$, depends on ϕ_v; For IW measurement, $\phi_s = 135°$).

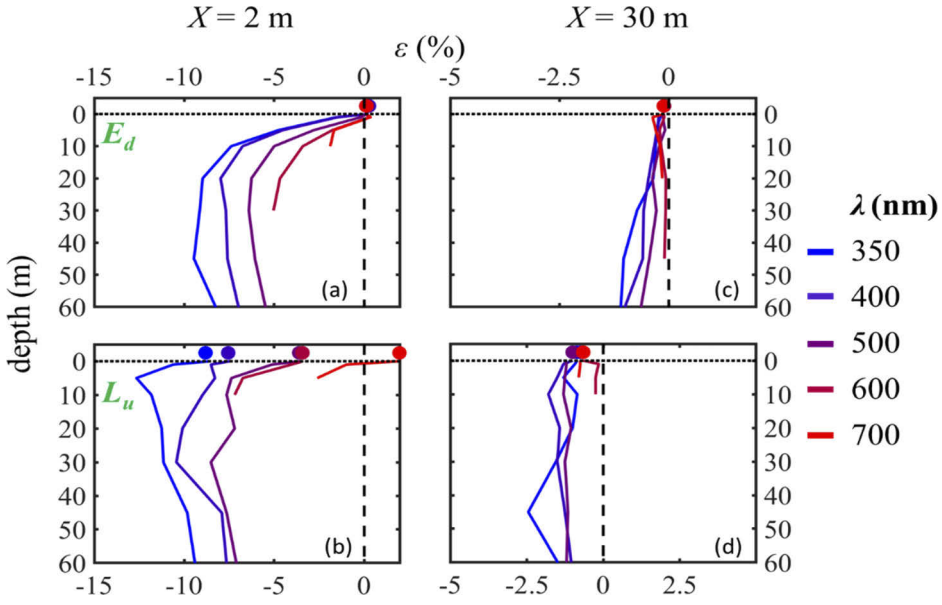

Fig. 10. Perturbation patterns for profiling measurements for water with 0.1 mg m^{-3} chlorophyll concentration ($\theta_s = 30°$, $\phi_s = 0°$).

Table 2. Parameters applied for case-1 water MC runs with 0.1 mg m^{-3} chlorophyll concentration

λ (nm)	r_{sky} (%), $\theta_s = 30°$	a (m^{-1})	b (m^{-1})	b_b (m^{-1})
350	56.6	0.024	0.126	0.009
400	44.1	0.017	0.107	0.006
500	30.9	0.029	0.082	0.003
600	23.8	0.226	0.067	0.002
700	19.3	0.627	0.057	0.001

Optics EXPRESS

For these simulations, ship size varies from a large vessel (i.e., 60 m by 15 m by 10 m) to a small boat (i.e., 5 m by 1 m by 1 m), R_{hull} and R_{draft} ranges from 10% to 50% and 2.5% to 12.5%, respectively.

The same "case-1" water and the wavelength dependent r_{sky} are applied (Table 2). Also, to better distinguish between X_s applied to a floating system and a profile system, the X_s for these two systems is represented as X_f and Xp, respectively hereafter. The minimum X_f, X_p and θ_v to achieve a threshold of 3% for L_w measurements are presented in Table 3. Because the perturbation at 350 nm is more severe than that at other wavelengths due to the strong skylight contributions (Fig. 10), the X_f, X_p and θ_v value that satisfy the threshold for 350 nm also satisfy the same threshold for the other wavelengths (i.e., 700 nm). Therefore, only the required X_f, X_p and θ_v at 350 nm is presented (Table 3).

Table 3. Minimum X_s (X_f and X_p) or θ_v to make $|\varepsilon_{Lw}|$ below 3% (λ = 350 nm)

Dimensions of the ship	R_{hull}: 10% R_{draft}: 2.5%		R_{hull}: 20% R_{draft}: 5%		R_{hull}: 30% R_{draft}: 7.5%		R_{hull}: 50% R_{draft}: 12.5%	
L; W; H; D (m)	X_f ; X_p (m)	θ_v (°)	X_f ; X_p (m)	θ_v (°)	X_f ; X_p (m)	θ_v (°)	X_f ; X_p (m)	θ_v (°)
60; 15; 10; 4	20; 30	50	20; 25	50	20; 25	50	18; 25	50
30; 10; 5; 2	12; 18	45	12; 18	50	12; 15	50	12; 15	50
20; 5; 3; 1	9; 12	45	9; 12	45	9; 12	40	9; 12	40
10; 3; 2; 1	3; 4	40	3; 4	40	3; 4	40	3; 3	30
5; 1; 1; 0.5	1; 1	30	1; 1	30	1; 1	30	1; 1	20

It was found that an X_f value around 2 to 3-times of the ship height could keep $|\varepsilon_{Lw}|$ under 3% (i.e., X_f = 30 m is able to keep $|\varepsilon_{Lw}|$ below 3% for an operational ship like Okeanos Explorer with H = 10 m). The value of X_p appears always larger because the negative perturbation increases with depth. The minimum values for X_f, X_p and θ_v appeared to decrease when the ship's reflectivity increases. This is because the maximum negative perturbation is on the short wavelength (as showed in Fig. 10) where the skylight contribution is strong (i.e., r_{sky} = 56.3% for λ = 350 nm). When the reflectance of the ship increases, higher reflected light from the hull compensates for the loss due to the blocking skylight by ship hull and consequently, results in lower minimum values of X_f, X_p and θ_v to achieve a threshold of $|\varepsilon_{Lw}|$. If focusing on wavelength with less skylight contribution (i.e., 700 nm), the minimum value of X_f, X_p and θ_v will be higher for a brighter ship hull due to strong perturbation from the ship hull reflectance.

It was also found that when the ship size changes from small to large (e.g., H from 1 m to 10 m), θ_v increases from 30° to 50° (θ_v is suggested to be 50° in Hooker and Morel [43]). The required θ_v would be higher if the ship is larger or having a stricter threshold for $|\varepsilon_{Lw}|$ (i.e., 1%). Although it is possible to take L_w measurements at larger viewing angles (i.e., $\theta_v \geq 60°$), such θ_v would raise the contribution of surface reflected light from the above-water approach, which would cause larger uncertainties in the derived L_w (Mobley [30], Lee *et al.* [32]).

For AW measurements, however, there are commonly applied setups that could reduce the ship perturbation such as extending the setups out of the deck (e.g., bow/stern) or deploying at the higher altitude of the deck (i.e., the top of the ship). These setups are equivalent to making the measurements farther away from the ship, then the required θ_v could be lower. For the ship shared similar size with Okeanos Explorer and with R_{hull} = 10%, if the setups could be deployed 5 m higher (15 m from the water surface), the required θ_v for the 3% threshold will be shifted from 50° to 45°. The last but not the least, most of the bows are not flat and big as that assumed for the cubic ship. The calculated perturbation could be slightly overestimated for the

Optics EXPRESS

AW measurements taken on the bow. Nevertheless, the difference due to the configuration of the bow is not significant. The result for the AW measurements (the suggested θ_v) is still robust.

5. Conclusions

The perturbations of an operating ship on radiance and irradiance in oceanic environments are re-evaluated via MC simulations by considering a cube "ship" with ship height and ship reflectance. It is found that the distance off the ship and the sky condition are the two most important factors. More severe perturbations were found under overcast sky than under clear sky, and IOPs change generally resulted in ~5% difference in perturbations on radiometric measurements. However, the changes of ship height resulted in significant differences on ship perturbations, which fill a gap of the previous studies. Under clear sky conditions, for water with chlorophyll concentration as 0.1 mg m^{-3} and assuming "Case-1" bio-optical relationships, for a ship with sizes similar as Okeanos Explorer (60 m by 15 m by 10 m), it is required to have an above-water radiometer over the front side viewing the water at ~50° from nadir, or a floating instrument ~20 m away the ship, or a profiling instrument ~25 m away the ship in order to limit ship's perturbation under ± 3%. As a rule of thumb, for floating instruments (i.e., the Skylight-Blocked Approach (SBA)), the $|\varepsilon_{Lw}|$ will be within 3% if the sensor can be deployed away from the ship at a distance around 3-times of ship's height. On the other hand, the radiometer over the ship's side having a viewing angle 30° to 50° from nadir (depending on the size of ship and the setups) is required to limit the ship's perturbation on $|\varepsilon_{Lw}|$ under 3%.

Funding

National Oceanic and Atmospheric Administration (NA11OAR4320199); University of Massachusetts; National Natural Science Foundation of China (41776184); National Aeronautics and Space Administration (80NSSC18K0509).

Acknowledgments

The authors thank the Massachusetts Green High Performance Computing Cluster for providing computation resources for this study. Comments and suggestions from two anonymous reviewers greatly improved this manuscript.

References

1. C. R. McClain, "A decade of satellite ocean color observations," Annu. Rev. Mar. Sci. **1**(1), 19–42 (2009).
2. W. W. Gregg and M. E. Conkright, "Decadal changes in global ocean chlorophyll," Geophys. Res. Lett. **29**(15), 20 (2002).
3. T. S. Moore, J. W. Campbell, and M. D. Dowell, "A class-based approach to characterizing and mapping the uncertainty of the MODIS ocean chlorophyll product," Remote Sens. Environ. **113**(11), 2424–2430 (2009).
4. J. E. O'Reilly, S. Maritorena, B. G. Mitchell, D. A. Siegel, K. L. Carder, S. A. Garver, M. Kahru, and C. McClain, "Ocean color chlorophyll algorithms for SeaWiFS," J. Geophys. Res.: Oceans **103**(C11), 24937–24953 (1998).
5. D. Antoine, F. d'Ortenzio, S. B. Hooker, G. Bécu, B. Gentili, D. Tailliez, and A. J. Scott, "Assessment of uncertainty in the ocean reflectance determined by three satellite ocean color sensors (MERIS, SeaWiFS and MODIS-A) at an offshore site in the Mediterranean Sea (BOUSSOLE project)," J. Geophys. Res.: Oceans **113**(C7), C07013 (2008).
6. M. Wang and S. Son, "VIIRS-derived chlorophyll-a using the ocean color index method," Remote Sens. Environ. **182**, 141–149 (2016).
7. D. Antoine, J. M. André, and A. Morel, "Oceanic primary production: 2. Estimation at global scale from satellite (coastal zone color scanner) chlorophyll," GBioC **10**(1), 57–69 (1996).
8. Z. Lee, J. Marra, M. J. Perry, and M. Kahru, "Estimating oceanic primary productivity from ocean color remote sensing: A strategic assessment," J. Mar. Syst. **149**, 50–59 (2015).
9. M. L. Zoffoli, Z. Lee, and J. F. Marra, "Regionalization and Dynamic Parameterization of Quantum Yield of Photosynthesis to Improve the Ocean Primary Production Estimates from Remote Sensing," Front. Mar. Sci. **5**, 446 (2018).
10. R. P. Stumpf, "Applications of satellite ocean color sensors for monitoring and predicting harmful algal blooms," Hum. Ecol. Risk Assess. **7**(5), 1363–1368 (2001).

Optics EXPRESS

11. D. L. Tang, H. Kawamura, H. Doan-Nhu, and W. Takahashi, "Remote sensing oceanography of a harmful algal bloom off the coast of southeastern Vietnam," J. Geophys. Res.: Oceans **109**, C03014 (2004).
12. Y.-H. Ahn and P. Shanmugam, "Detecting the red tide algal blooms from satellite ocean color observations in optically complex Northeast-Asia Coastal waters," Remote Sens. Environ. **103**(4), 419–437 (2006).
13. M. J. Sayers, A. G. Grimm, R. A. Shuchman, K. R. Bosse, G. L. Fahnenstiel, S. A. Ruberg, and G. A. Leshkevich, "Satellite monitoring of harmful algal blooms in the Western Basin of Lake Erie: A 20-year time-series," J. Great Lakes Res. **45**(3), 508–521 (2019).
14. H. R. Gordon and M. Wang, "Retrieval of water-leaving radiance and aerosol optical thickness over the oceans with SeaWiFS: a preliminary algorithm," Appl. Opt. **33**(3), 443–452 (1994).
15. C. Hu, K. L. Carder, and F. E. Muller-Karger, "Atmospheric correction of SeaWiFS imagery over turbid coastal waters: a practical method," Remote Sens. Environ. **74**(2), 195–206 (2000).
16. K. G. Ruddick, F. Ovidio, and M. Rijkeboer, "Atmospheric correction of SeaWiFS imagery for turbid coastal and inland waters," Appl. Opt. **39**(6), 897–912 (2000).
17. M. Wang and W. Shi, "Estimation of ocean contribution at the MODIS near-infrared wavelengths along the east coast of the US: Two case studies," Geophys. Res. Lett. **32**(17), L13606 (2005).
18. M. Wang, "Remote sensing of the ocean contributions from ultraviolet to near-infrared using the shortwave infrared bands: simulations," Appl. Opt. **46**(9), 1535–1547 (2007).
19. M. Wang and W. Shi, "The NIR-SWIR combined atmospheric correction approach for MODIS ocean color data processing," Opt. Express **15**(24), 15722–15733 (2007).
20. M. Wang, J. Tang, and W. Shi, "MODIS-derived ocean color products along the China east coastal region," Geophys. Res. Lett. **34**(6), L06611 (2007).
21. M. Wang, S. Son, and W. Shi, "Evaluation of MODIS SWIR and NIR-SWIR atmospheric correction algorithms using SeaBASS data," Remote Sens. Environ. **113**(3), 635–644 (2009).
22. L. Jiang and M. Wang, "Improved near-infrared ocean reflectance correction algorithm for satellite ocean color data processing," Opt. Express **22**(18), 21657–21678 (2014).
23. C. D. Mobley, J. Werdell, B. Franz, Z. Ahmad, and S. Bailey, "Atmospheric correction for satellite ocean color radiometry," Tech. Report, NASA/TM-2016-217551 (2016).
24. J. L. Mueller, C. Davis, R. Arnone, R. Frouin, K. Carder, Z. Lee, R. Steward, S. Hooker, C. D. Mobley, and S. McLean, "Above-water radiance and remote sensing reflectance measurements and analysis protocols," in *Ocean Optics Protocols for Satellite Ocean Color Sensor Validation* (NASA, 2000), pp. 98–107.
25. J. L. Mueller, "In-water radiometric profile measurements and data analysis protocols," in *Ocean Optics Protocols for Satellite Ocean Color Sensor Validation* (NASA, 2003), pp. 7–20.
26. S. B. Hooker, G. Lazin, G. Zibordi, and S. McLean, "An evaluation of above-and in-water methods for determining water-leaving radiances," JAtOT **19**, 486–515 (2002).
27. J. Mueller, J. Mueller, C. Pietras, S. Hooker, D. Clark, A. M. R. Frouin, B. Mitchell, R. Bidigare, C. Trees, and J. Werdell, *Ocean Optics Protocols For Satellite Ocean Color Sensor Validation, Revision 3, volumes 1 and 2* (NASA, 2002), p. 210004.
28. M. Ondrusek and V. P. Lance, "Report for Dedicated JPSS VIIRS Ocean Color Calibration/Validation Cruise," Tech. Rep. (National Oceanic and Atmospheric Administration, 2015).
29. G. Zibordi, F. Mélin, S. B. Hooker, D. D'Alimonte, and B. Holben, "An autonomous above-water system for the validation of ocean color radiance data," IEEE Trans. Geosci. Remote Sensing **42**, 401–415 (2004).
30. C. D. Mobley, "Estimation of the remote-sensing reflectance from above-surface measurements," Appl. Opt. **38**(36), 7442–7455 (1999).
31. K. G. Ruddick, K. Voss, A. C. Banks, E. Boss, A. Castagna, R. Frouin, M. Hieronymi, C. Jamet, B. C. Johnson, and J. Kuusk, "A Review of Protocols for Fiducial Reference Measurements of Downwelling Irradiance for the Validation of Satellite Remote Sensing Data over Water," Remote Sens. **11**(15), 1742 (2019).
32. Z. Lee, Y.-H. Ahn, C. Mobley, and R. Arnone, "Removal of surface-reflected light for the measurement of remote-sensing reflectance from an above-surface platform," Opt. Express **18**, 26313–26324 (2010).
33. J. J. Cullen, A. M. Ciotti, and M. R. Lewis, "Observing biologically induced optical variability in coastal waters," in *Ocean Optics XII* (International Society for Optics and Photonics, 1994), pp. 105–115.
34. Z. Lee, N. Pahlevan, Y.-H. Ahn, S. Greb, and D. O'Donnell, "Robust approach to directly measuring water-leaving radiance in the field," Appl. Opt. **52**(8), 1693–1701 (2013).
35. L. Satlantic, "Operation Manual for the HyperOCR," Halifax, Nova Scotia (2004).
36. H. R. Gordon, "Ship perturbation of irradiance measurements at sea. 1: Monte Carlo simulations," Appl. Opt. **24**(23), 4172–4182 (1985).
37. J. Piskozub, "Effect of ship shadow on in-water irradiance measurements," Oceanologia **46**, 103–112 (2004).
38. G. Zibordi, J. P. Doyle, and S. B. Hooker, "Offshore tower shading effects on in-water optical measurements," JAtOT **16**(11), 1767–1779 (1999).
39. J. P. Doyle and G. Zibordi, "Optical propagation within a three-dimensional shadowed atmosphere–ocean field: application to large deployment structures," Appl. Opt. **41**(21), 4283–4306 (2002).
40. K. Voss, J. Nolten, and G. Edwards, "Ship shadow effects on apparent optical properties," in *Ocean Optics VIII* (International Society for Optics and Photonics, 1986), pp. 186–191.

Optics EXPRESS

41. R. W. Spinrad and E. A. Widder, "Ship shadow measurements obtained from a manned submersible," in *Ocean Optics XI* (International Society for Optics and Photonics, 1992), pp. 372–384.
42. C. T. Weir, D. A. Siegel, A. F. Michaels, and D. W. Menzies, "In-situ evaluation of a ship's shadow," in *Ocean Optics XII* (International Society for Optics and Photonics, 1994), pp. 815–822.
43. S. B. Hooker and A. Morel, "Platform and environmental effects on above-water determinations of water-leaving radiances," JAtOT **20**(1), 187–205 (2003).
44. S. B. Hooker, E. R. Firestone, G. Zibordi, J.-F. Berthon, D. DAlimonte, D. vanderLinde, and J. W. Brown, "Tower-perturbation measurements in above-water radiometry," Tech. Rep. (NASA, 2003).
45. N. Ship, "Okeanos Explorer," (Readiness Report, 2012).
46. G. R. Fournier and M. Jonasz, "Computer-based underwater imaging analysis," in *SPIE's International Symposium on Optical Science, Engineering, and Instrumentation* (International Society for Optics and Photonics, 1999), pp. 62–70.
47. G. R. Fournier and J. L. Forand, "Analytic phase function for ocean water," in *Ocean Optics XII* (International Society for Optics and Photonics, 1994), pp. 194–202.
48. R. A. Leathers, T. V. Downes, C. O. Davis, and C. D. Mobley, "Monte Carlo radiative transfer simulations for ocean optics: a practical guide," (DTIC Document, 2004).
49. Z. Shang, Z. Lee, Q. Dong, and J. Wei, "Self-shading associated with a skylight-blocked approach system for the measurement of water-leaving radiance and its correction," Appl. Opt. **56**(25), 7033–7040 (2017).
50. C. D. Mobley, B. Gentili, H. R. Gordon, Z. Jin, G. W. Kattawar, A. Morel, P. Reinersman, K. Stamnes, and R. H. Stavn, "Comparison of numerical models for computing underwater light fields," Appl. Opt. **32**(36), 7484–7504 (1993).
51. K. J. Waters, R. C. Smith, and M. R. Lewis, "Avoiding ship-induced light-field perturbation in the determination of oceanic optical properties," Oceanog **3**(2), 8–21 (1990).
52. W. S. Helliwell, G. N. Sullivan, B. Macdonald, and K. J. Voss, "Ship shadowing: model and data comparisons," in *Ocean Optics X* (International Society for Optics and Photonics, 1990), pp. 55–72.
53. E. Aas, "Two-stream irradiance model for deep waters," Appl. Opt. **26**(11), 2095–2101 (1987).
54. W. W. Gregg and K. L. Carder, "A simple spectral solar irradiance model for cloudless maritime atmospheres," Limnol. Oceanogr. **35**(8), 1657–1675 (1990).